Ezh2 variant orchestrates cholesterol biosynthesis via epigenetic regulation in mouse cerebellum

Fei Guan [1,2,3†], Zongyan Jiang[1,2,3†], Ye Tian[1,2,3], Bijun Jiang[1,2,3], Yixian Fan[1,2,3], Huamin Liang[1,2,3], Jing Jin[4*], Ying Yin[1,2,3,5*], Ximiao He[1,2,3,5*]

[1] Department of Physiology, School of Basic Medical Science, Huazhong University of Science and Technology, Wuhan 430030, Hubei, China.
[2] Center for Genomics and Proteomics Research, School of Basic Medicine, Tongji Medical College, Huazhong University of Science and Technology, Wuhan 430030, Hubei, China
[3] Hubei Key Laboratory of Drug Target Research and Pharmacodynamic Evaluation, Huazhong University of Science and Technology, Wuhan 430030, Hubei, China.
[4] National Demonstration Center for Experimental Basic Medical Education, School of Basic Medicine, Tongji Medical College, Huazhong University of Science and Technology, Wuhan 430030, China;
[5] Key Laboratory of Vascular Aging, Ministry of Education, Tongji Hospital, Tongji Medical College, Huazhong University of Science and Technology, Wuhan 430030, Hubei, China

[†]These authors have contributed equally to this work.
*** Correspondence:**
Corresponding Authors
Ximiao He: XimiaoHe@hust.edu.cn
Ying Yin: YinYing@hust.edu.cn
Jing Jin: JinJng@hust.edu.cn

Running title: *Ezh2* variant in cerebellar cholesterol metabolism

Keywords: cerebellum, *Ezh2*, alternative splicing, multi-omics, epigenetics, cholesterol, astroglia

Abstract

Alternative splicing is highly prevalent and evolutionarily conserved in the brain, contributing to neuronal diversity and function. The chromatin modifier enhancer of zeste homolog 2 (EZH2) undergoes extensive splicing, but the functional significance of exon 3 donor site selection in the adult brain remains unclear. In this study, we identify the exon 3 long isoform of *Ezh2* (*Ezh2*^{Long}) as a cerebellum-enriched isoform with an important role in neurological function. Loss of *Ezh2*^{Long} reduces the expression of cholesterol biosynthesis genes and lowers cerebellar cholesterol levels, in association with increased H3K27me3-mediated repression at SREBP2-targeted promoters. *Ezh2*^{Long} deficiency disrupts astroglial cholesterol homeostasis and myelination, accompanied by neurological abnormalities. Notably, cholesterol restoration via valproic acid (VPA) treatment ameliorates myelination and behavioral deficits in *Ezh2*$^{Long-/-}$ mice. In summary, our findings identify *Ezh2*^{Long} as a critical regulator of cerebellar cholesterol metabolism and highlight the importance of *Ezh2* alternative splicing in maintaining cerebellar homeostasis and neurological function.

Dear Editor,

Polycomb-mediated chromatin regulation is essential for establishing and maintaining gene expression programs in the central nervous system (CNS). As the catalytic core of polycomb repressive complex 2 (PRC2), enhancer of zeste homolog 2 (EZH2) catalyzes trimethylation of histone H3 at lysine 27 (H3K27me3), thereby promoting chromatin compaction and gene silencing[1]. EZH2 plays indispensable roles in neural development and function, including balancing neural progenitor self-renewal and differentiation[2], regulating lineage specification[3], and supporting neural circuit maturation across developmental stages[4]. It has also been implicated in adult neurogenesis and neural plasticity[5], underscoring its broad and context-dependent influence in the nervous system. Alternative splicing provides an additional layer of post-transcriptional regulation by generating distinct mRNA and protein isoforms from a single gene. Given its high prevalence and evolutionary conservation in the brain[6], splicing-mediated isoform diversity may fine-tune EZH2 function in a region- and cell-type-dependent manner.

Multiple *Ezh2* splice isoforms have been reported and linked to distinct biological contexts. An adult tissue-expressed isoform, EZH2β, shares core properties with canonical EZH2 yet displays divergent gene targeting[7]. A brain-associated variant, *Ezh2*-X9, has been implicated in neuronal proliferation and differentiation in rats[8]. Alternative processing involving exon 3 truncation and exon 14 skipping has also been observed across multiple tissues[9]. Notably, exon 14 skipping in spermatocytes reduces H3K27me3 while favoring H3K27me2 and impacts differentiation programs[9]. Our previous work further demonstrated that exclusive expression of *Ezh2* variant with exon 3 truncation disrupts oocyte mitochondrial function and compromises female fertility[10]. Together, these findings support the concept that *Ezh2* isoforms are not merely redundant products, but can encode functionally distinct regulatory states. Despite these advances, most mechanistic insight into *Ezh2* splicing has come from proliferative or developmental contexts, leaving open whether isoform-specific *Ezh2* programs shape adult brain homeostasis.

Here, we focus on an evolutionarily conserved alternative donor usage event at the 3' end of *Ezh2* exon 3 that generates two isoforms, exon 3 long isoform ($Ezh2^{Long}$) and exon 3 short isoform ($Ezh2^{Short}$), which respectively contain or lack a 27-nt region encoding a 9-amino-acid segment. We find that $Ezh2^{Long}$ is highly enriched in the cerebellum. Using an $Ezh2^{Long}$-specific knockout ($Ezh2^{Long-/-}$) mouse model combined with multi-omics analyses, we found that $Ezh2^{Long}$ contributes to cerebellar cholesterol metabolism via balanced epigenetic regulation of SREBP2-dependent cholesterol biosynthetic programs, highlighting its important role in cerebellar homeostasis and neurological function.

Alternative donor sites within exon 3 of *Ezh2* are evolutionarily conserved across mammals, including humans, pan troglodytes, and mice (Fig. S1A). Analysis of RNA-seq datasets revealed broad *Ezh2* expression across brain regions, with pronounced enrichment in the cerebellum (Fig. S1B). Reverse transcription-quantitative PCR (RT-qPCR) confirmed this regional enrichment, with the highest *Ezh2* mRNA abundance detected in the cerebellum (Fig. 1A), while western blot analysis showed a similar regional trend in total EZH2 protein levels (Fig. S1C). Isoform-specific analysis further showed that the $Ezh2^{Long}$ predominated across examined brain regions and was particularly

enriched in the cerebellum (Fig. 1B), indicating preferential representation of this isoform in cerebellar tissue. We therefore focused on the cerebellum to investigate the isoform-specific function of *Ezh2*^{Long}. *Ezh2*$^{Long-/-}$ mice were generated as previously describe[10] (Fig. S1D-E). RT-qPCR confirmed complete loss of *Ezh2*^{Long}, accompanied by increased *Ezh2*^{Short} and a net reduction in total *Ezh2* mRNA (Fig. 1C-D). Despite these transcript-level changes, total EZH2 protein abundance remained comparable between wild-type (WT) and mutant mice (Fig. S1F), suggesting compensatory regulation at the protein level. *Ezh2*$^{Long-/-}$ mice exhibited partial developmental lethality (Fig. S1G), and surviving adults displayed reduced body weight and brain size, while the brain-to-body weight ratio remained comparable to WT littermates (Fig. S1H-J).

To determine the molecular consequences of *Ezh2*^{Long} deficiency, we performed RNA sequencing (RNA-seq) of cerebellar tissues from WT and *Ezh2*$^{Long-/-}$ mice. Transcriptomic profiling revealed modest global transcriptional changes, with 368 genes significantly upregulated and 205 genes significantly downregulated (Fig. 1E). Gene set enrichment analysis (GSEA) revealed activation of immune-related signaling and marked suppression of cholesterol biosynthesis in *Ezh2*$^{Long-/-}$ mice (Fig. 1F). Gene Ontology Biological Process (GO-BP) enrichment analysis supported these findings and additionally identified learning behavior and myelination among the downregulated pathways (Fig. S2A). Notably, the expression of most enzymes involved in endogenous cholesterol biosynthesis was reduced (Fig. S2B), which was further validated by RT-qPCR and western blotting (Fig. 1G-H). To determine whether this transcriptional suppression resulted in corresponding metabolic alterations, we performed targeted quantitative sterolomics using mass spectrometry. Multiple sterol intermediates, together with free cholesterol, were significantly decreased in *Ezh2*$^{Long-/-}$ cerebella (Fig. 1I). Consistently, total cholesterol levels were reduced in the cerebellum and hippocampus, but remained unchanged in other brain regions and plasma (Fig. S2C-D), indicating a region-selective effect of *Ezh2*^{Long} deficiency on brain cholesterol homeostasis.

To determine how loss of *Ezh2*^{Long} suppresses the cholesterol biosynthetic program, we performed upstream regulator analysis, which identified sterol regulatory element-binding protein 2 (SREBP2) and its regulatory factors SCAP and SPRING1 among the most strongly predicted inactivated regulators (Fig. 1J). However, western blot analysis showed comparable levels of both full-length and processed active SREBP2 between WT and *Ezh2*$^{Long-/-}$ mice (Fig. 1K), suggesting that *Ezh2*^{Long} deletion may primarily affect the transcriptional regulatory activity of SREBP2 rather than its protein abundance or processing. Given the canonical histone methyltransferase function of EZH2, we hypothesized that the impaired SREBP2 transcriptional program might involve altered chromatin regulation. Global H3K27me3 and Histone H3 lysine 27 acetylation (H3K27ac) levels remained largely unchanged between WT and *Ezh2*$^{Long-/-}$ cerebella (Fig. S2E). We therefore examined locus-specific chromatin alterations by performing cleavage under targets and tagmentation followed by sequencing (CUT&Tag-seq) for SREBP2, H3K27me3, and H3K27ac, together with assay for transposase accessible chromatin using sequencing (ATAC-seq). At SREBP2 target genes, *Ezh2*^{Long} deficiency was associated with reduced SREBP2 occupancy, H3K27ac, and chromatin accessibility, accompanied by increased H3K27me3 (Fig. S2F). We next focused on genes involved in cholesterol biosynthesis and found that chromatin accessibility was negatively correlated with H3K27me3 enrichment but positively correlated with SREBP2 occupancy (Fig. 1L). Supporting this notion, aggregate analysis of SREBP2-bound cholesterol

synthesis genes revealed increased H3K27me3 and concomitant decreases in H3K27ac, chromatin accessibility, and SREBP2 binding around their transcription start sites (TSS) in *Ezh2*$^{Long-/-}$ mice (Fig. 1M-N). These chromatin changes were accompanied by reduced transcription of the corresponding genes, with representative loci showing concordant alterations across CUT&Tag-seq, ATAC-seq, and RNA-seq datasets (Fig. S2G). Collectively, these findings indicate that *Ezh2*^{Long} contributes to maintaining a balanced chromatin state at SREBP2-regulated cholesterol biosynthesis genes. Shifting the isoform balance toward *Ezh2*^{Short} following *Ezh2*^{Long} deletion is associated with a more repressive chromatin configuration, reduced SREBP2 occupancy, and diminished transcriptional output.

To characterize cellular heterogeneity and metabolic states in *Ezh2*$^{Long-/-}$ cerebella, we performed single-nucleus RNA sequencing (snRNA-seq) of WT and *Ezh2*$^{Long-/-}$ mice (Fig. 2A). Unsupervised clustering identified 17 transcriptionally distinct clusters representing seven major cerebellar cell types based on canonical marker expression, including glutamatergic and GABAergic neurons, astroglia, oligodendrocytes, vascular cells, ependymal cells, and immune cells (Fig. 2B, S3A). Cell-type-specific analysis revealed the most pronounced transcriptional alterations in neurons and astroglia (Fig. S3B). Notably, astroglia, the main suppliers of brain cholesterol, showed significantly reduced expression of key cholesterol biosynthesis genes (*Nsdhl*, *Fdft1*, *Msmo1*, *Hmgcs1*, and *Cyp51*) (Fig. S3C), accompanied by suppression of the cholesterol biosynthesis pathway as revealed by GSEA (Fig. 2C). To further assess cell-type-specific metabolic changes, we applied single-cell flux estimation analysis (scFEA) to the snRNA-seq data. *Ezh2*$^{Long-/-}$ mice showed reduced metabolic flux through the downstream sterol synthesis route from (E,E)-Farnesyl-PP to Cholesterol, whereas the upstream reaction (Acetyl-CoA-to-(E,E)-Farnesyl-PP) was less affected (Fig. 2D). This reduction was most prominent in astroglia, particularly astrocytes and Bergmann glia, consistent with the decreased expression of cholesterol biosynthetic enzymes (Fig. 2D-E). Together, these analyses suggest that impaired cholesterol synthesis in astroglia may contributes substantially to the metabolic phenotype associated with *Ezh2*^{Long} deficiency.

To further resolve the cellular basis of impaired cholesterol metabolism in astroglia, we reclustered astroglial cells and identified seven subpopulations with distinct genotype distributions (Fig. 2F). Notably, two Bergmann glia-enriched clusters showed striking genotype bias: AST4 was derived almost exclusively from WT mice, whereas AST5 was predominantly represented in *Ezh2*$^{Long-/-}$ mice, implying that *Ezh2*^{Long} loss is associated with a distinct Bergmann glial state (Fig. 2F). Among the astroglial subclusters, AST5 exhibited the lowest activity of sterol synthesis (Fig. 2G), which may underscore its impaired capacity for cholesterol biosynthesis. To assess differentiation status in the genotype-biased Bergmann glial populations, we conducted CytoTRACE analysis. Astroglia from *Ezh2*$^{Long-/-}$ mice showed relatively lower differentiation potential than WT mice, with the lowest potential observed in the AST5 subtype (Fig. S3D), prompting further investigation of premature aging-related changes. GSEA subsequently revealed significant activation of senescence-associated pathways in mutant astroglia (Fig. S3E). Moreover, we observed a robust upregulation of the cellular senescence markers, particularly in AST5 subpopulation (Fig. 2H). Aged astrocytes have been reported to exhibit reduced cholesterol synthesis and enhanced cholesterol transport[11,12], adopting a neuroinflammatory A1-like reactive phenotype[13]. As shown above, AST5 showed reduced cholesterol anabolic activity and enhanced cholesterol transport relative to AST4, together with

senescence-like and A1-like reactive signatures (Fig. S3F). We therefore sought to validate these findings experimentally in primary cerebellar astrocytes isolated from WT and *Ezh2*$^{Long-/-}$ mice (Fig. S3G-H). Consistent with the transcriptomic analyses, astrocytes from *Ezh2*$^{Long-/-}$ mice exhibited reduced expression of cholesterol biosynthetic genes and increased expression of senescence markers, and showed lower free cholesterol levels than WT controls (Fig. 2I-K). Taken together, these findings identify a mutant-enriched Bergmann glial state characterized by impaired cholesterol biosynthesis and senescence-associated features. Given the comparable cell numbers and proportions of AST4 and AST5, the minimal cholesterol anabolic capacity of AST5 may substantially contribute to the disrupted cholesterol homeostasis observed in the *Ezh2*$^{Long-/-}$ cerebellum.

We next considered the potential consequences of this disrupted cholesterol homeostasis for myelination and neurological function. Oligodendrocytes envelop neuronal axons with myelin, a specialized cholesterol-rich membrane essential for proper neuronal function and normal learning and memory. Consistent with this close dependence on cholesterol, western blot analysis revealed reduced levels of myelin structural proteins in the cerebellum of *Ezh2*$^{Long-/-}$ mice compared with WT controls (Fig. S4A). We further evaluated the functional consequences of *Ezh2*^{Long} deficiency using a series of behavioral assays. Although exploratory locomotor activity was comparable between groups, *Ezh2*$^{Long-/-}$ mice spent less time in the center of the open field and, in the elevated plus maze, less time in the open arms but more time in the closed arms, indicating increased anxiety-like behavior (Fig. 2N-O, S4B-E). Mutant mice also displayed impaired recognition and spatial memory, as evidenced by reduced novel object preference and poorer performance during the probe trial of Morris water maze test (MWMT) (Fig. 2P-Q, S4F-I). To explore whether improving cholesterol metabolism could alleviate these phenotypes, we treated *Ezh2*$^{Long-/-}$ mice with valproic acid (VPA) (Fig. 2L), which has been reported to promote cholesterol biosynthesis by restoring the astrocyte-associated Bloch pathway and alleviate experimental demyelination[14]. VPA treatment significantly increased cerebellar total cholesterol levels in mutant mice and partially restored the reduced levels of myelin structural proteins (Fig. 2M, S4A). Importantly, these molecular improvements were accompanied by improved behavioral performance. Compared with *Ezh2*$^{Long-/-}$ mice, VPA-treated mutants spent more time in the center of the open field and, in the elevated plus maze, more time in the open arms but less time in the closed arms (Fig. 2N-O, S4B-E). Cognitive performance was likewise improved by VPA, with greater novel object preference, increased time in the target quadrant and more platform crossings during the probe trial (Fig. 2P-Q, S4F-I). These results suggest that restoration of brain cholesterol homeostasis may help ameliorate myelin decline and neurobehavioral deficits associated with *Ezh2*^{Long} deficiency.

Alternative splicing expands the functional diversity of *Ezh2*, yet the isoform-specific roles of exon 3 splice variants in the adult brain remain poorly understood. In this study, we identified *Ezh2*^{Long} as a cerebellum-enriched splice isoform and found that its loss was associated with impaired cholesterol biosynthesis, altered myelination, and neurological abnormalities. Integrated transcriptomic and epigenomic analyses further linked suppression of cholesterol biosynthetic genes to altered chromatin states and reduced SREBP2 occupancy, revealing an isoform-dependent mechanism connecting *Ezh2* alternative splicing to cerebellar cholesterol homeostasis.

EZH2 is best known as the catalytic component of PRC2, which mediates transcriptional repression through H3K27 trimethylation, but it can also exert non-canonical transcriptional regulatory functions across different biological contexts. Previous studies have shown that EZH2 regulates cholesterol biosynthesis in a PRC2-dependent manner by modulating H3K27me3 at promoters of cholesterol synthesis genes, including SQLE in head and neck squamous cell carcinoma[15] and DHCR24 in granulosa-lutein cells[16]. In our study, loss of *Ezh2*^{Long} did not markedly alter total EZH2 protein or global H3K27me3 and H3K27ac levels, but was associated with increased H3K27me3, reduced H3K27ac and chromatin accessibility, and decreased SREBP2 occupancy at cholesterol biosynthesis genes. These findings are consistent with the involvement of canonical PRC2-associated chromatin regulation in SREBP2-dependent transcription and support a model in which increased H3K27me3 restricts chromatin accessibility required for transcriptional activation. EZH2 can also regulate cholesterol metabolism independently of PRC2. For instance, EZH2 cooperates with AR and AR-V7 to regulate cholesterol metabolic genes in prostate cancer[17], while a recent study identified a non-canonical EZH2-SREBP2 axis that promotes cholesterol biosynthesis in multiple cancer types[18].

Such context dependence may also involve *Ezh2* isoform-specific regulation. A recent study showed that the 9-aa insertion in EZH2^{Long} strengthens PRC2 association and confers a greater effect on endogenous H3K27me3 than EZH2^{Short}[19]. Notably, *Ezh2*^{Long} depletion has been reported to increase H3K27me3 at selected loci, an effect proposed to involve compensatory activity of residual *Ezh2*^{Short}, highlighting isoform-specific regulation during embryonic development. This locus-specific behavior is consistent with our observation in the cerebellum that *Ezh2*^{Long} deletion is accompanied by compensatory *Ezh2*^{Short} upregulation and a more repressive chromatin configuration at SREBP2 target genes despite unchanged global H3K27me3. These findings suggest that the resulting shift in isoform composition may be insufficient to preserve local chromatin states and instead alter locus-specific chromatin regulation. Thus, the balance between *Ezh2*^{Long} and *Ezh2*^{Short} may contribute to chromatin regulation and SREBP2-dependent transcription at cholesterol biosynthesis genes.

scFEA revealed a marked barrier to cholesterol biosynthetic flux in astroglia, particularly in mutant-enriched AST5, in *Ezh2*$^{Long-/-}$ mice. Although we validated reduced cholesterol synthesis in primary astrocytes isolated from mouse cerebellum, isolating the specific AST5 subpopulation for direct functional assessment remains challenging. Astroglia are a major source of cholesterol in the brain, and impaired cholesterol synthesis can compromise neurite growth, synaptic function, and myelination. Thus, the neurological abnormalities observed in *Ezh2*$^{Long-/-}$ mice may, at least in part, result from disrupted cholesterol synthesis in astroglia.

The functional relevance of cholesterol dysregulation was further supported by pharmacological rescue. VPA, a histone deacetylase inhibitor, is widely used as an antiepileptic agent for managing seizures and epilepsy. In addition to its primary clinical applications, VPA has been reported to modulate cholesterol homeostasis. Restoration of *Ezh2*$^{Long-/-}$ cerebellar cholesterol levels through VPA treatment enhanced myelin structural protein biogenesis and ameliorated neurobehavioral deficits. Although VPA has pleiotropic effects and cholesterol restoration may not be its sole mechanism of action, the concordant improvement in cholesterol metabolism, myelination, and behavioral phenotypes supports a contribution of impaired cholesterol homeostasis to the

neurological consequences of *Ezh2*$^{Long-/-}$ deficiency.

In conclusion, our findings reveal an isoform-specific role of *Ezh2* in the regulation of cerebellar cholesterol metabolism. *Ezh2*^{Long} contributes to maintaining an appropriate epigenetic landscape at SREBP2-regulated cholesterol biosynthesis genes. Loss of *Ezh2*^{Long} shifts the isoform balance toward *Ezh2*^{Short} and is associated with a more repressive configuration at SREBP2 target loci, reduced transcriptional output of cholesterol biosynthetic genes, and disrupted glial cholesterol homeostasis (Fig. 2R). These findings reveal a novel layer of regulation by *Ezh2* alternative splicing and establish a link between epigenetic remodeling and lipid metabolic homeostasis in the cerebellum.

References

1. Cao, R., Wang, L., Wang, H., Xia, L., Erdjument-Bromage, H., Tempst, P., Jones, R.S., and Zhang, Y. (2002). Role of histone H3 lysine 27 methylation in Polycomb-group silencing. Science *298*, 1039-1043.
2. Pereira, J.D., Sansom, S.N., Smith, J., Dobenecker, M.-W., Tarakhovsky, A., and Livesey, F.J. (2010). Ezh2, the histone methyltransferase of PRC2, regulates the balance between self-renewal and differentiation in the cerebral cortex. Proc Natl Acad Sci U S A *107*, 15957-15962. 10.1073/pnas.1002530107.
3. Hirabayashi, Y., Suzki, N., Tsuboi, M., Endo, T.A., Toyoda, T., Shinga, J., Koseki, H., Vidal, M., and Gotoh, Y. (2009). Polycomb limits the neurogenic competence of neural precursor cells to promote astrogenic fate transition. Neuron *63*, 600-613. 10.1016/j.neuron.2009.08.021.
4. Qi, C., Liu, S., Qin, R., Zhang, Y., Wang, G., Shang, Y., Wang, Y., and Liang, J. (2014). Coordinated regulation of dendrite arborization by epigenetic factors CDYL and EZH2. J Neurosci *34*, 4494-4508. 10.1523/JNEUROSCI.3647-13.2014.
5. Zhang, J., Ji, F., Liu, Y., Lei, X., Li, H., Ji, G., Yuan, Z., and Jiao, J. (2014). Ezh2 regulates adult hippocampal neurogenesis and memory. J Neurosci *34*, 5184-5199. 10.1523/JNEUROSCI.4129-13.2014.
6. Merkin, J., Russell, C., Chen, P., and Burge, C.B. (2012). Evolutionary dynamics of gene and isoform regulation in Mammalian tissues. Science *338*, 1593-1599. 10.1126/science.1228186.
7. Grzenda, A., Lomberk, G., Svingen, P., Mathison, A., Calvo, E., Iovanna, J., Xiong, Y., Faubion, W., and Urrutia, R. (2013). Functional characterization of EZH2β reveals the increased complexity of EZH2 isoforms involved in the regulation of mammalian gene expression. Epigenetics Chromatin *6*, 3. 10.1186/1756-8935-6-3.
8. Li, D., Wang, H.-L., Huang, X., Gu, X., Xue, W., and Xu, Y. (2019). Identification and Functional Characterization of a New Splicing Variant of EZH2 in the Central Nervous System. Int J Biol Sci *15*, 69-80. 10.7150/ijbs.28129.
9. Mu, W., Starmer, J., Yee, D., and Magnuson, T. (2018). EZH2 variants differentially regulate polycomb repressive complex 2 in histone methylation and cell differentiation. Epigenetics Chromatin *11*, 71. 10.1186/s13072-018-0242-9.
10. Guo, S.-M., Liu, X.-P., Tian, Q., Fei, C.-F., Zhang, Y.-R., Li, Z.-M., Yin, Y., He, X., and Zhou, L.-Q. (2022). Regulatory roles of alternative splicing at Ezh2 gene in mouse oocytes.

Reproductive Biology and Endocrinology : RB&E *20*, 99. 10.1186/s12958-022-00962-x.

11. Boisvert, M.M., Erikson, G.A., Shokhirev, M.N., and Allen, N.J. (2018). The Aging Astrocyte Transcriptome from Multiple Regions of the Mouse Brain. Cell Rep *22*, 269-285. 10.1016/j.celrep.2017.12.039.
12. Saher, G. (2023). Cholesterol Metabolism in Aging and Age-Related Disorders. Annu Rev Neurosci *46*, 59-78. 10.1146/annurev-neuro-091922-034237.
13. Clarke, L.E., Liddelow, S.A., Chakraborty, C., Münch, A.E., Heiman, M., and Barres, B.A. (2018). Normal aging induces A1-like astrocyte reactivity. Proc Natl Acad Sci U S A *115*, E1896-E1905. 10.1073/pnas.1800165115.
14. Zhu, X., Yao, Y., Hu, Y., Yang, J., Zhang, C., He, Y., Zhang, A., Liu, X., Zhang, C., and Gan, G. (2021). Valproic acid suppresses cuprizone-induced hippocampal demyelination and anxiety-like behavior by promoting cholesterol biosynthesis. Neurobiol Dis *158*, 105489. 10.1016/j.nbd.2021.105489.
15. Xu, X., Chen, J., Li, Y., Yang, X., Wang, Q., Wen, Y., Yan, M., Zhang, J., Xu, Q., Wei, Y., et al. (2021). Targeting epigenetic modulation of cholesterol synthesis as a therapeutic strategy for head and neck squamous cell carcinoma. Cell Death Dis *12*, 482. 10.1038/s41419-021-03760-2.
16. Li, H., Shen, J., Ma, S., Zhao, F., Zhao, W., Chen, F., Fu, Y., Li, B., Cheng, J., and Deng, Y. (2023). TGF-β1 suppresses de novo cholesterol biosynthesis in granulosa-lutein cells by down-regulating DHCR24 expression via the GSK-3β/EZH2/H3K27me3 signaling pathway. Int J Biol Macromol *224*, 1118-1128. 10.1016/j.ijbiomac.2022.10.196.
17. Wang, J., Park, K.-S., Yu, X., Gong, W., Earp, H.S., Wang, G.G., Jin, J., and Cai, L. (2022). A cryptic transactivation domain of EZH2 binds AR and AR's splice variant, promoting oncogene activation and tumorous transformation. Nucleic Acids Res *50*, 10929-10946. 10.1093/nar/gkac861.
18. Kim, A., Pan, B., Yu, X., Gao, X., Khudaverdyan, N., Taherian, F., Xu, C., Zhong, H., Xiong, Y., Kaniskan, H.Ü., et al. (2026). An EZH2-SREBP2 axis promotes cholesterol biosynthesis and represents a noncanonical vulnerability in tumorigenesis. Nat Cell Biol. 10.1038/s41556-026-02048-x.
19. Guo, N., Guo, Q., Zhan, H., Lv, J., Fang, Y., Li, J., Wang, J., Li, D., Ma, X., Yan, Q., and Wang, Z. (2025). EZH2 variants derived from cryptic splice sites govern distinct epigenetic patterns during embryonic development. Nucleic Acids Res *53*. 10.1093/nar/gkaf869.

Figure and Legends

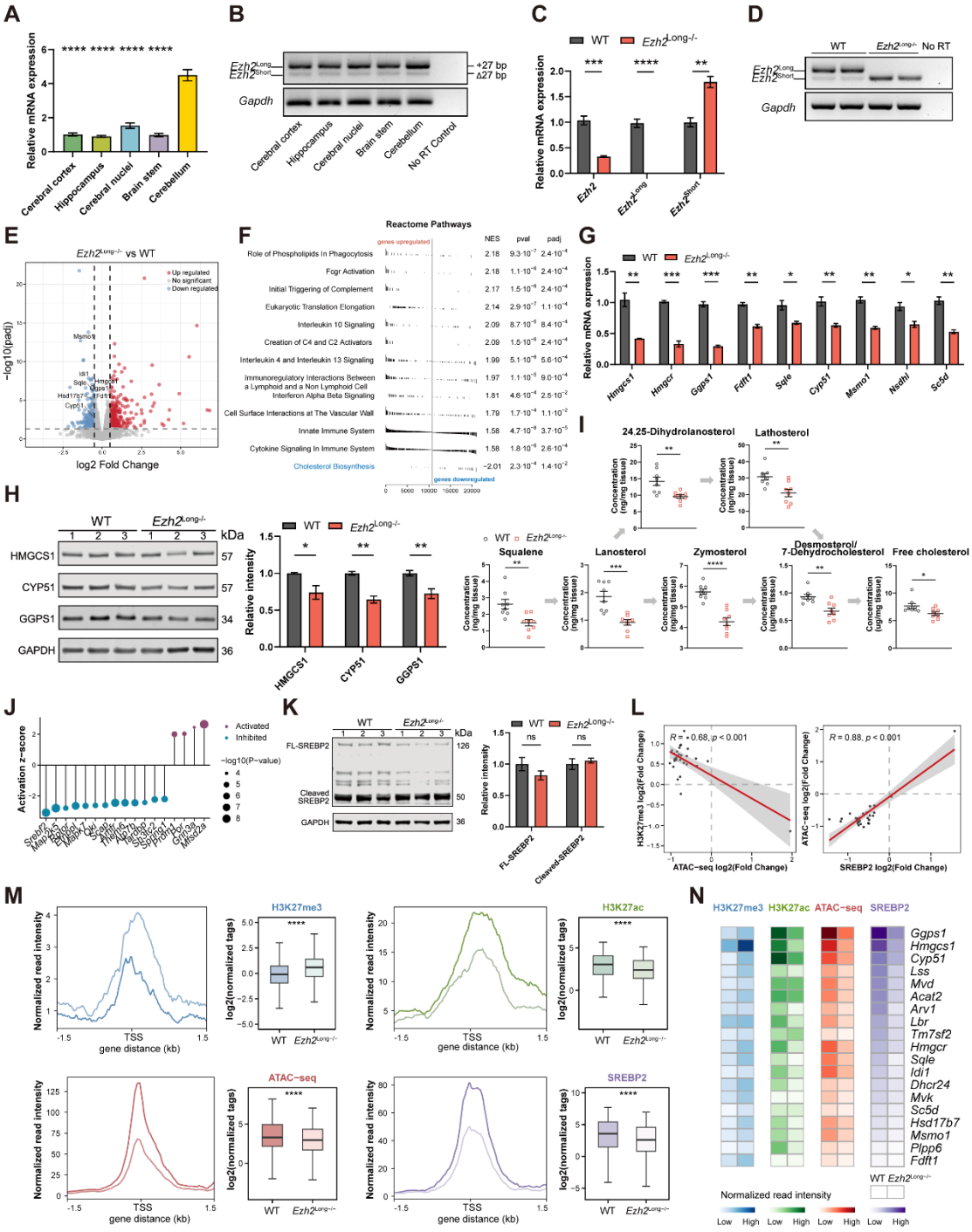

Figure 1. ***Ezh2*$^{\text{Long}}$ deficiency impairs cerebellar cholesterol biosynthesis through epigenetic alteration of SREBP2-dependent transcription.**

(A) RT-qPCR analysis of *Ezh2* mRNA expression in different brain regions of WT (n = 3) mice. One-way ANOVA; ****$p < 0.0001$. **(B)** RT-qPCR results of the *Ezh2* exon 3 alternative splicing event in multiple brain regions of WT mouse. **(C-D)** *Ezh2* transcript expression in the cerebellum of WT and *Ezh2*$^{\text{Long-/-}}$ mice detected by RT-qPCR **(C)** and representative images of PCR products visualized on agarose gels **(D)**. Unpaired t test; **$p < 0.01$; ***$p < 0.001$; ****$p < 0.0001$. **(E)** Volcano plot showing the DEGs between WT and *Ezh2*$^{\text{Long-/-}}$ mice. The significantly upregulated genes are marked in red and significantly downregulated genes are marked in blue. **(F)** Enriched Reactome pathways analysis of *Ezh2*$^{\text{Long-/-}}$ versus WT. Genes were ranked by expression fold change,

with the most upregulated genes at the top and downregulated genes at the bottom. **(G)** RT-qPCR results of the genes involved in cholesterol biosynthesis in isolated WT (n = 3) and *Ezh2*$^{Long-/-}$ (n = 3) cerebellums. Unpaired t test; *$p < 0.05$; **$p < 0.01$; ***$p < 0.001$. **(H)** Western blot analysis and quantification of the representative enzymes involved in cholesterol biosynthesis in isolated WT (n = 3) and *Ezh2*$^{Long-/-}$ (n = 3) cerebellums. GAPDH was used as loading control. Unpaired t test; *$p < 0.05$; **$p < 0.01$. **(I)** Quantification of sterol levels in cerebellums isolated from WT (n = 8) and *Ezh2*$^{Long-/-}$ (n = 8) mice. Unpaired t test; *$p < 0.05$; **$p < 0.01$; ***$p < 0.001$; ****$p < 0.0001$. **(J)** The top enriched upstream transcription regulators of the DEGs of RNA-seq data in *Ezh2*$^{Long-/-}$ mice. **(K)** Western blot analysis and quantification of SREBP2 in isolated WT (n = 3) and *Ezh2*$^{Long-/-}$ (n = 3) cerebellums. GAPDH was used as loading control. Unpaired t test; ns, not significant. **(L)** Correlation analysis of $\log_2$ fold changes (*Ezh2*$^{Long-/-}$ versus WT) for H3K27me3, ATAC-seq, and SREBP2 signals at promoter regions of cholesterol biosynthesis pathway. Left, correlation between H3K27me3 and ATAC-seq alterations; right, correlation between ATAC-seq and SREBP2 alterations. **(M)** Metagene plots (left) and boxplots (right) showing the average occupancies of CUT&Tag-seq (H3K27me3, H3K27ac and SREBP2) and ATAC-seq within ± 1.5 kb of the TSS for 19 SREBP2-bound cholesterol biosynthesis genes in WT and *Ezh2*$^{Long-/-}$ mice. Unpaired t test; ****$p < 0.0001$. **(N)** Heatmaps of the average occupancies of CUT&Tag-seq (H3K27me3, H3K27ac and SREBP2) and ATAC-seq within ± 1.5 kb from the TSS for 19 SREBP2 targeted genes involved in cholesterol biosynthesis in WT and *Ezh2*$^{Long-/-}$ mice.

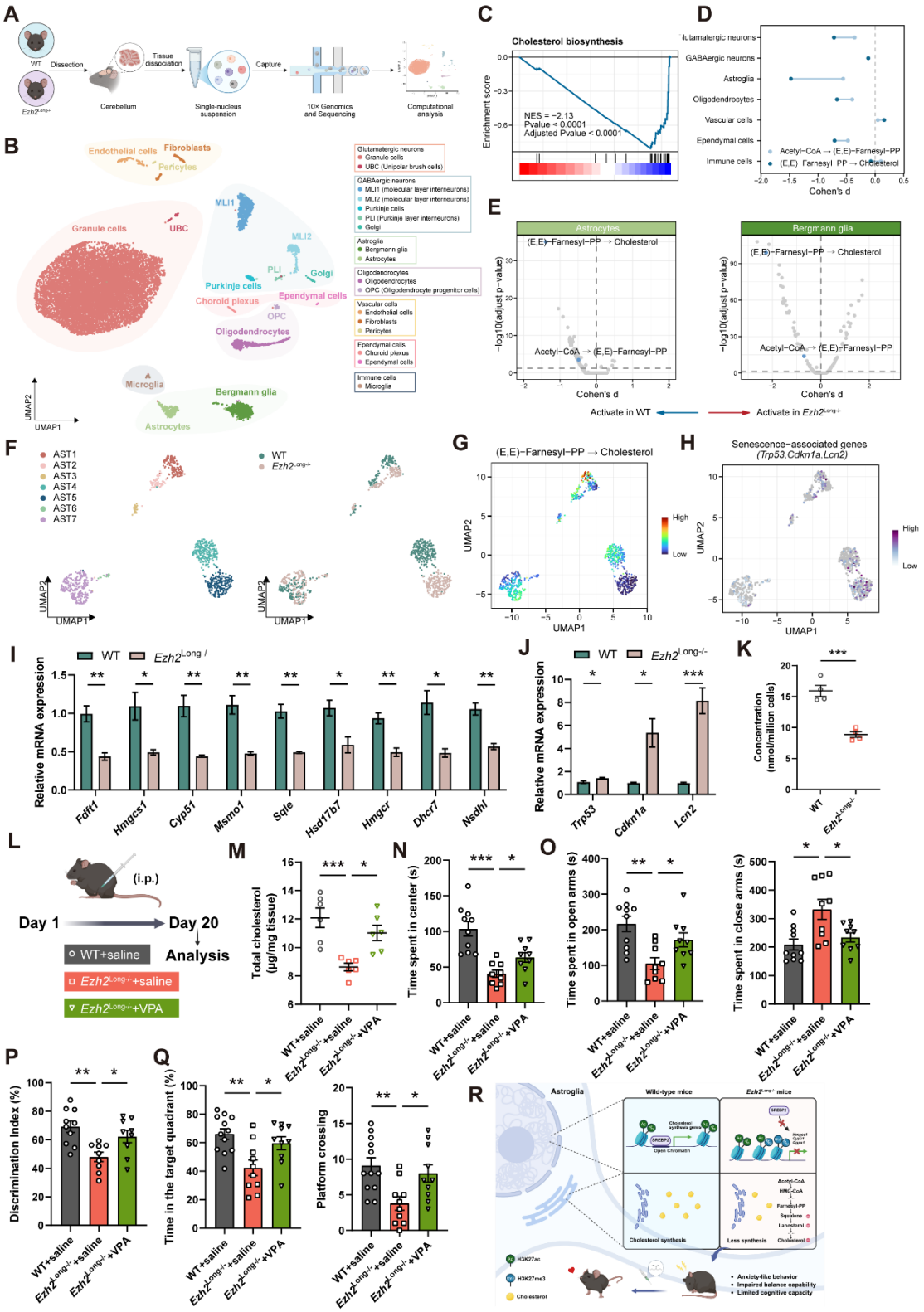

Figure 2. *Ezh2*^{Long} deficiency disrupts astroglial cholesterol homeostasis, with cholesterol deficiency-associated defects ameliorated by valproic acid.

(A) Schematic diagram representation of the experimental procedure, encompassing cerebellum isolation, single-cell dissociation, and droplet-based RNA sequencing and downstream bioinformatics analysis. **(B)** Uniform manifold approximation and projection (UMAP) visualization of 14,244 nuclei isolated from WT and *Ezh2*$^{Long-/-}$ murine cerebella, coloured by cell type identity.

Subtypes are grouped into broad cell types indicated by rectangles. **(C)** GSEA analysis of *Ezh2*$^{Long-/-}$ versus WT by using cholesterol biosynthesis signatures. Genes were ranked by expression fold change, with the most upregulated genes on the left side of the plot and downregulated genes on the right. **(D)** Dumbbell plot showing differential metabolic flux analysis of Acetyl-CoA-to-(E,E)-Farnesyl-PP (lightblue) and (E,E)-Farnesyl-PP-to-Cholesterol(darkblue) across different cell types between WT and *Ezh2*$^{Long-/-}$ mice. **(E)** Volcano plot showing differential metabolic flux analysis of metabolic reactions in astrocytes (left) and Bergmann glia (right) between WT and *Ezh2*$^{Long-/-}$ mice (Likelihood ratio test). The metabolic reactions of Acetyl-CoA-to-(E,E)-Farnesyl-PP and (E,E)-Farnesyl-PP-to-Cholesterol are marked in blue. **(F)** UMAP visualization of the subclusters of astroglia (left) and distribution of sample origin (right). **(G)** Feature plot of metabolic flux reaction for (E,E)-Farnesyl-PP-to-Cholesterol. Metabolic flux levels for each cell are color-coded and overlaid onto UMAP plot. **(H)** Feature plot of combined expression distribution for senescence marker genes. Expression levels for each cell are color-coded and overlaid onto UMAP plot. **(I)** RT-qPCR results of the genes involved in cholesterol biosynthesis in isolated WT (n = 3) and *Ezh2*$^{Long-/-}$ (n = 3) primary astrocytes. Unpaired t test; *$p < 0.05$; **$p < 0.01$. **(J)** RT-qPCR results of the senescence marker genes in isolated WT (n = 4) and *Ezh2*$^{Long-/-}$ (n = 4) primary astrocytes. Unpaired t test; *$p < 0.05$; ***$p < 0.001$. **(K)** Quantification of free cholesterol levels in primary astrocytes isolated from WT (n = 4) and *Ezh2*$^{Long-/-}$ (n = 4) mice. Unpaired t test; ***$p < 0.001$. **(L)** Schematic illustration of valproic acid or saline solution administered via intraperitoneal injection every 48 h for a total of 10 administrations. **(M)** Quantification of total cholesterol levels in cerebellum from saline-treated WT (n = 6), saline-treated *Ezh2*$^{Long-/-}$ (n = 6) and VPA-treated *Ezh2*$^{Long-/-}$ (n = 6) mice. One-way ANOVA; *$p < 0.05$; ***$p < 0.001$. **(N)** Time spent in the center of the open field arena by saline-treated WT, saline-treated *Ezh2*$^{Long-/-}$, and VPA-treated *Ezh2*$^{Long-/-}$ mice (WT + saline, n = 10; *Ezh2*$^{Long-/-}$ + saline, n = 9; *Ezh2*$^{Long-/-}$ + VPA, n = 9). One-way ANOVA; ns, not significant; *$p < 0.05$; ***$p < 0.001$; ****$p < 0.0001$. **(O)** Time spent in the open and closed arms of the elevated plus maze by saline-treated WT, saline-treated *Ezh2*$^{Long-/-}$, and VPA-treated *Ezh2*$^{Long-/-}$ mice (WT + saline, n = 10; *Ezh2*$^{Long-/-}$ + saline, n = 9; *Ezh2*$^{Long-/-}$ + VPA, n = 9). One-way ANOVA; ns, not significant; *$p < 0.05$; **$p < 0.01$; ****$p < 0.0001$. **(P)** Discrimination index during the test phase of the novel object recognition test (NORT) in saline-treated WT, saline-treated *Ezh2*$^{Long-/-}$, and VPA-treated *Ezh2*$^{Long-/-}$ mice (WT + saline, n = 10; *Ezh2*$^{Long-/-}$ + saline, n = 9; *Ezh2*$^{Long-/-}$ + VPA, n = 9). One-way ANOVA; *$p < 0.05$; **$p < 0.01$. **(Q)** Percentage of time spent in the target quadrant and number of platform crossings during the probe trial of MWMT in saline-treated WT, saline-treated *Ezh2*$^{Long-/-}$, and VPA-treated *Ezh2*$^{Long-/-}$ mice (WT + saline, n = 12; *Ezh2*$^{Long-/-}$ + saline, n = 10; *Ezh2*$^{Long-/-}$ + VPA, n = 10). One-way ANOVA; ns, not significant; *$p < 0.05$; **$p < 0.01$. **(R)** Schematic representation of the epigenetic mechanism by which *Ezh2*^{Long} deficiency impairs SREBP2-dependent cholesterol biosynthesis.